Cascaded H-Bridge Multilevel Inverter System Fault Diagnosis Using a PCA and Multiclass Relevance Vector Machine Approach

Tianzhen Wang, Hao Xu, Jingang Han, Elhoussin Elbouchikhi, *Member, IEEE*, and Mohamed El Hachemi Benbouzid, *Senior Member, IEEE*

***Abstract*—Multilevel inverters, for their distinctive performance, have been widely used in high voltage and high-power applications in recent years. As power electronics equipment reliability is very important and to ensure multilevel inverter systems stable operation, it is important to detect and locate faults as quickly as possible. In this context and to improve fault diagnosis accuracy and efficiency of a cascaded H-bridge multilevel inverter system (CHMLIS), a fault diagnosis strategy based on the principle component analysis and the multiclass relevance vector machine (PCA-mRVM), is elaborated and proposed in this paper. First, CHMLIS output voltage signals are selected as input fault classification characteristic signals. Then, a fast Fourier transform is used to preprocess these signals. PCA is used to extract fault signals features and to reduce samples dimensions. Finally, an mRVM model is used to classify faulty samples. Compared to traditional approaches, the proposed PCA-mRVM strategy not only achieves higher model sparsity and shorter diagnosis time, but also provides probabilistic outputs for every class membership. Experimental tests are carried out to highlight the proposed PCA-mRVM diagnosis performances.**

***Index Terms*—Cascaded H-bridge, fault diagnosis, model sparsity, principal component analysis (PCA), multiclass relevance vector machine (mRVM).**

NOMENCLATURE

CHMLIS	Cascaded H-bridge multilevel inverter system.
SPWM	Sinusoidal pulse width modulation.
OC	Open circuits.
SC	Short circuits.
H1S1	H-bridge 1, Switch 1.
FFT	fast Fourier transform.
PCA	Principle component analysis.
mRVM	Multiclass relevance vector machine.
BP	Back propagation neural network.
SVM	Support vector machine.

Manuscript received July 4, 2014; revised September 29, 2014 and November 26, 2014; accepted January 5, 2015. Date of publication January 16, 2015; date of current version August 21, 2015. This work was supported in parts by the National High-Tech Research and Development Program of China (NO. 2013A2041106), the National Natural Science Foundation of China (NO.61203089 and 61304186), and Innovation Key Project of Shanghai Municipal Education Commission (NO.14ZZ141). Recommended for publication by Associate Editor M. Saeedifard.

T.-Z. Wang, H. Xu, and J.-G Han are with the Department of Electrical Automation, Shanghai Maritime University, 201306 Shanghai, China (e-mail: wtz0@sina.com; bodhi319@gmail.com; jghan@shmtu.edu.cn).

E. Elbouchikhi is with ISEN Brest, EA 4325 LBMS, 29200 Brest, France (e-mail: El-houssin.Elbouchikhi@isen.fr).

M.E.H. Benbouzid is with the University of Brest, EA 4325 LBMS, 29238 Brest, France (e-mail: Mohamed.Benbouzid@univ-brest.fr).

Color versions of one or more of the figures in this paper are available online at http://ieeexplore.ieee.org.

Digital Object Identifier 10.1109/TPEL.2015.2393373

I. INTRODUCTION

INDUSTRY is requiring higher power ratings in the recent years. Multilevel inverters, as converters new type, have been widely applied in the field of high voltage and high-power field since they become a solution for high-power applications [1]–[2]. Compared to a traditional two-level inverter, the multilevel itself possesses the following advantages: low voltage stress in power switches; series voltage sharing of power devices [3]–[5]; output voltage waveform low harmonic content; less electromagnetic interference; less switching loss; high working efficiency. In addition, the multilevel inverter not only produces high power ratings, but also enables the use of renewable energy sources [6]. Cascaded H-bridge multilevel inverter systems (hereinafter called the CHMLISs) have availability as a key feature allowing good application prospects [7]. Thus, it is now widely applied in the field of high-power transformers [8]. Troubled by the extensive use of the power semiconductor devices, the probability of multilevel inverter fault is increasingly rising, such as open circuits (OC) or short circuits (SC) of the power switch transistors [9]. Since the multilevel inverter systems are applied in high-power applications, the system reliability of the power electronics equipment is very important [10]. In the area of industrial applications, for instance, the industrial manufacturing depends heavily on the induction motor and its inverter system for process control [11]. As we all know, the downtime of manufacturing equipment will cause a great loss of more than hundreds to thousands of dollars per hour. Therefore, the fault detection and diagnosis are vital for enterprises production line [12]. In order to protect the circuit and to reduce the influence of power devices failure, some protective circuits have been applied to the inverter system, such as, overheating, overcurrent, and overload relays [13]. These protective circuits may fail too. This may be due to several reasons such as several nonlinear factors in the multilevel inverter, the complex circuit configuration, the non-normal use, power system disturbance, load disturbance, and electromagnetic interference [14]. Hence, a fault detection and diagnosis procedure will help diagnosing and locating the faults of the inverter [15].

In order to keep normal operation for the multilevel inverter system, the expertise of fault behaviors, fault prediction and fault diagnosis will be necessary. Fault diagnosis of power electronic devices includes the following two aspects: one is fault information acquirement, which means obtaining the information when the fault occurs using certain fault detection approach, another is fault diagnosis and classification, which are based on

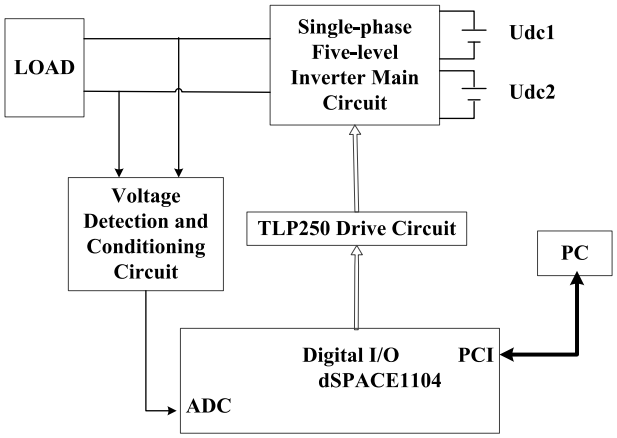

Fig. 1. CHMLIS configuration.

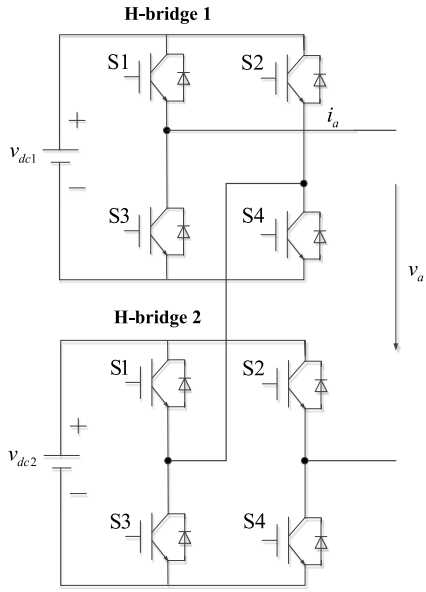

Fig. 2. Single-phase cascaded five-level inverter.

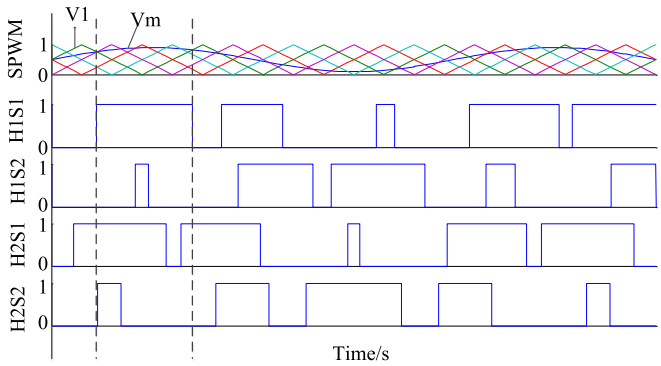

Fig. 3. SPWM scheme digital implementation.

the detected faults information to diagnose the type and localization of faults by a certain fault diagnosis approach [9]. In this particular context, faults should be quickly detected after the occurrence. If an inverter system runs continuously under the abnormal conditions, this would cause other failures and bring serious consequences [16]. Moreover, the CHMLIS consists of many switching devices, so its system is complex with many nonlinear factors [17]. In the case of a fault, it is difficult to diagnose the fault in time by the conventional approaches. Therefore, some innovative diagnosis approaches are necessary in CHMLIS, which can not only deal with the nonlinear detection problems but also diagnose and locate the faults quickly.

Regarding the CHMLIS, depending on the faults type and locations, the system voltage and current will be different correspondingly. In order to judge fault type and location more quickly and effectively, many researchers usually focus on the system output current or voltage, and then, generalize a series of fault diagnosis approaches from the study [18] and [19]. Lots of diagnosis approaches have been used for the inverters [20]–[25]. An optimal fault-tolerant control technique is proposed for open-circuit faults in five-phase permanent-magnet synchronous machine drives in [26]. Open-circuit faults in stator windings of the machine as well as inverter switches have been analyzed in this paper. A technique based on a recent enhancement on wavelets, which is known as complex wavelets, is proposed in [27] for identifying multiple faults in vector controlled induction motor drives. Radial, axial, and tangential vibrations are analyzed for diagnostic purpose. To solve the complex problems in multilevel inverters, Bordignon has proposed the slope method, which is based on the use of the slope of the diameter of the current space vector trajectory for fault detection [28]. A real-time inverter fault diagnosis approach is proposed, which is based on the subtractive clustering analysis of the stator current vector and a quick mean current vector calculation in [29]. The approach detects the fault within 1/4 cycle and have been applied in various control strategies. However, it is infeasible to apply this approach on some other topologies. Besides, a fault diagnosis approach based on a fuzzy support vector machine is proposed in [30]. Although this method achieves better diagnosis accuracy, the diagnosis computing time is much longer than other approaches.

To improve the accuracy and efficiency of CHMLIS fault diagnosis, this paper proposes PCA-mRVM strategy, which has higher model sparsity for fault diagnosis. The proposed diagnosis strategy could find fault location from CHMLIS output voltage waveform. First, to make the fault signature obvious, the fast Fourier transform (FFT) of the sampled data is computed in order to extract the frequency domain of the signals [31], [32]. Then, the PCA method is used to reduce the data dimension and extract signal features [33]. Finally, the mRVM method is used to classify and locate the faults, which has a model of high sparse degree, output the probability of all kinds of members, and can solve the nonlinear problem [34]. In order to verify the effectiveness of the proposed PCA-mRVM strategy, a CHMLIS fault diagnosis experiment test bench is built based on dSPACE1104 real-time control system. The proposed approach has been compared to traditional diagnosis strategies based on experimental data.

In the following, Section II briefly introduces the fault diagnosis system. Section III illustrates the proposed fault diagnosis

TABLE I
FAULT TYPES AND CHMLIS DESCRIPTION

Fault types	Category	Description
Simple-fault, a total of nine classes.	1	Normal: Considers a special fault, which implies a total of one class.
	2	Only one device is faulty which means A total of eight classes.
Complicated-faults, a total of 28 classes.	3	Two devices of the same leg are faulty: A total of four classes.
	4	Two upper-leg (lower-leg) devices of one bridge are faulty: A total of four classes.
	5	Two diagonal devices of one bridge are faulty: A total of four classes.
	6	Two devices of different bridge are faulty: A total of 16 classes.

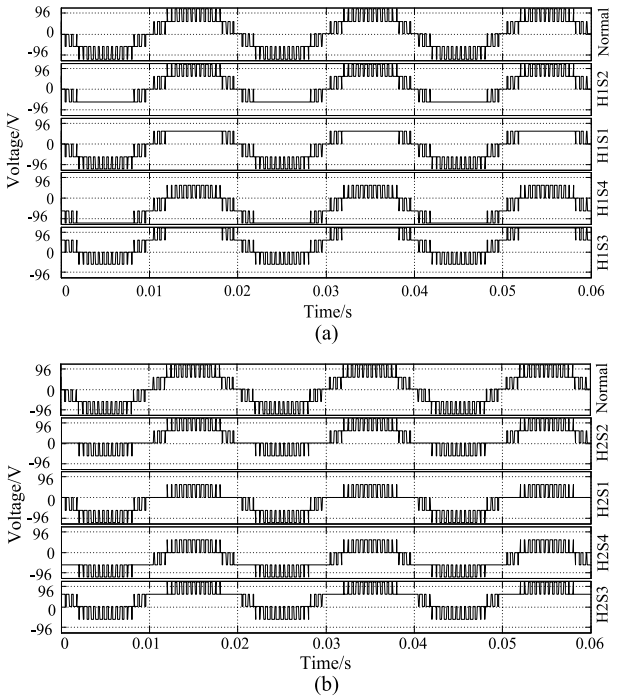

Fig. 4. Output waveform when Cascaded H-bridge switch S1-S4 open circuit. (a) Output waveform of H-bridge 1 open circuit, (b) Output waveform of H-bridge 2 open circuit.

strategy. Section IV details the experimental setup configuration and results analysis. Section V describes the simulation system and reports on some results. Finally, Section VI reports on some general conclusions and perspectives.

II. FAULT DIAGNOSIS SYSTEM

A. Configuration of Fault Diagnosis System

Fig. 1 shows the configuration of CHMLIS, which is presented in this paper. The system hardware consists of a single-phase five-level inverter, IGBT drive circuit, and a dSPACE1104 controller board. Besides, the voltage sensor has been used to measure the output voltage of the single-phase five-level inverter. This paper discusses the conditions where there is only one or two devices affected by OC fault at the same time. OC fault refers to the case where the power semiconductor device is under the off-state status. This status appears when the gate driver unit or the gate firing hardware circuit fails. The SC faults can be converted to OC faults by adding a fast acting fuse in the circle where the switch is. Thus, when SC faults happen, the fast acting fuse disconnects and the SC faults are converted to OC faults. Fig. 2 shows a single-phase cascaded five-level inverter topology.

The selection of the modulation strategy is generally based on the practical application as well as on the configuration of the hardware. The modulation mechanism in CHMLIS is commonly done through the switching mode of the adjustment switch, which makes the system working at the proximal electrical level status. Furthermore, each modulation strategy will produce different abnormal behaviors when a failure occurs on the hardware circuit. Thus, the comparative research between the abnormal behavior (in the presence of fault) and the normal behavior is a common approach of fault detection or postfault decision. Thus, it is necessary to choose an appropriate modulation strategy for the further development of fault detection and classification [35], [36].

In Fig. 3, V_m is the modulating reference signal and V_1 is the triangular carrier and the pulse signal. This paper adopts the carrier phase-shifted SPWM (CPS-SPWM) technology. The analysis and experiments have demonstrated that the technology possesses the advantages of high equivalent switching frequency, low switching losses, and fast dynamic response as well as wide bandwidth. Based on the aforementioned advantages, the technology is quite interesting to apply for different control strategies. Fig. 3 illustrates the process of generating pulse signals for IGBT drives. The value of the inverter output voltage is modulated by modulation index m_a [37]. Herein, m_a refers to the amplitude ratio of the carrier signal and the modulation signal. The *D*-value of carrier phase angle between adjacent modules is

$$\theta_d = (2\pi/k_c)/n \tag{1}$$

where k_c refers to the frequency ratio of the carrier signal and the modulation signal.

B. Fault Signal Analysis

The faults of CHMLIS generally fall into OC and SC of power switches. This paper mainly focuses on the OC faults. In the case of the SC faults, it can be converted into OC faults by implementing fast acting fuses into the inverter circuit. When SC faults happen, the fast acting fuse disconnects and the SC faults are converted to OC faults [38]. Some of the technical approaches, that are used to extract faults information from system, are needed to achieve fault type and fault localization. It is known that the probability of several transistors breakdown at the same time is very small. Thus, a maximum of two switching devices faults are discussed in this paper. The type of OC faults falls into single OC and double OC. Among them, the first one is defined as simple fault, and the second one is defined as complicated fault. The details of faults type are shown in Table I.

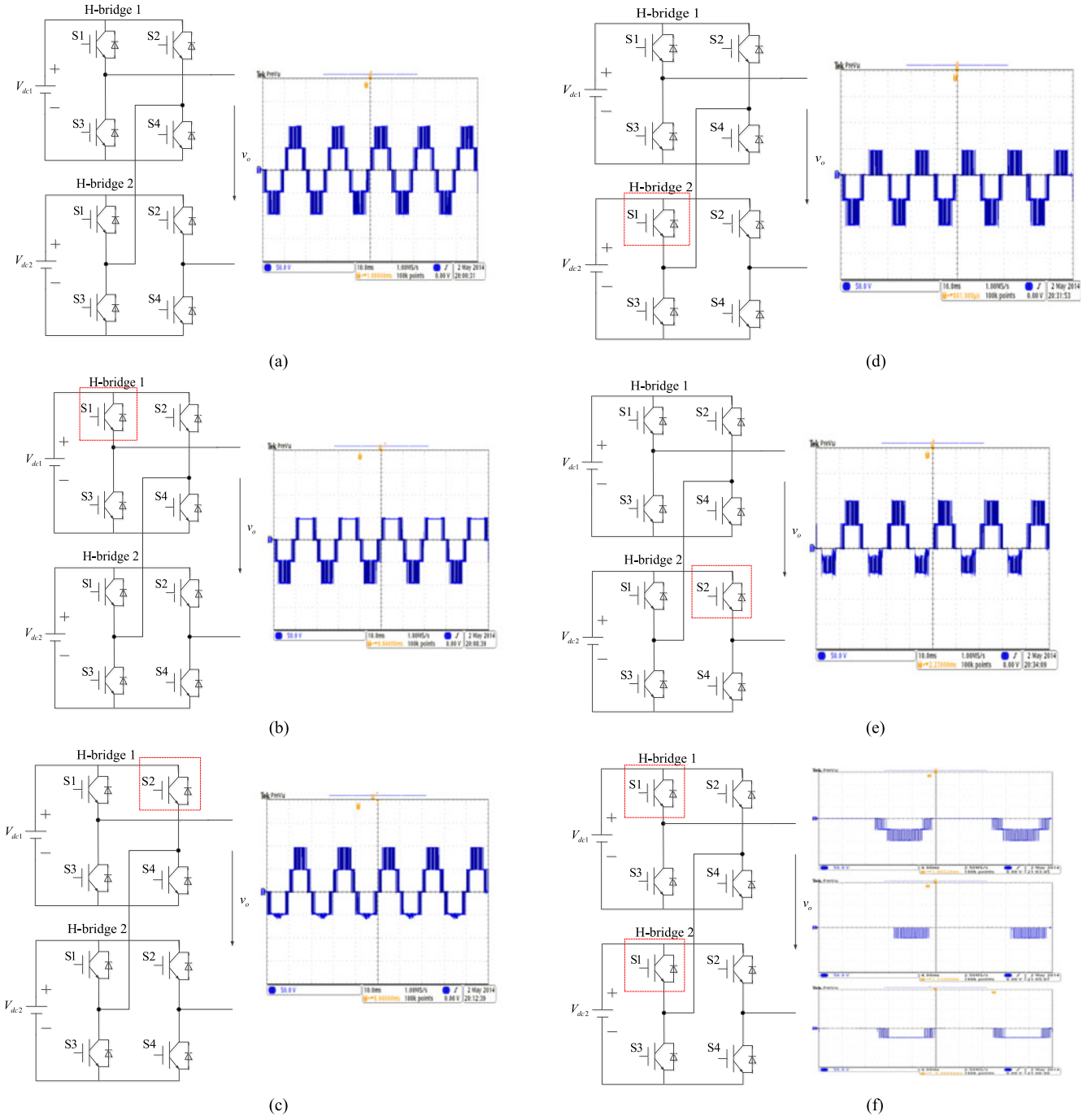

Fig. 5. Output voltage signals for different fault types. (a) Inverter work under normal state. (b) OC fault occurred in the inverter H1S1. (c) OC fault occurred in the inverter H1S2. (d) OC fault occurred in the inverter H2S1. (e) OC fault occurred in the inverter H2S2. (f) Complicated-faults of H1S1 and H2S1 OC.

It is very important to select the appropriate signals as an input of the classification diagnostic model, which will directly affect diagnostic results. Regarding, the inverter output current; it is affected by the effect of load variations and may lead to false diagnosis. Therefore, the inverter output voltage waveform, which can be acquired using a voltage measurement sensor at the inverter output terminals, is used in the present work. Indeed, the output voltage signals of CHMLIS are selected as characteristic signals input of the fault classification using the proposed fault diagnosis strategy.

Depending on the location of switch OC faults, the inverter output voltage waveforms will be different, as illustrated in Fig. 4. The output voltage waveforms are nearly the same when the faults appear at the same position. It can be concluded from this figure that the output voltage waveform is closely related to the fault location. It has been proven that, it is feasible to detect and locate the inverter simple fault with the inverter output voltage waveform, as illustrated in Fig. 5(a)–(e) [17]. However, it is difficult to distinguish the complicated faults by means of

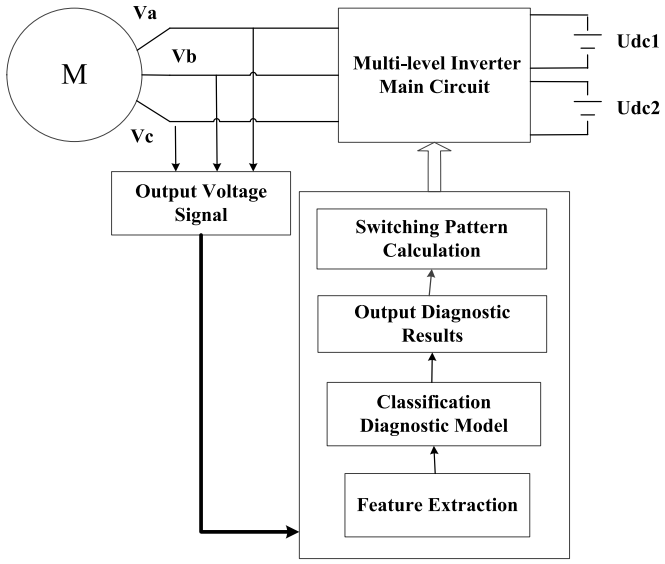

Fig. 6. Structure of the fault diagnosis strategy.

the output voltage of system. In this paper, three voltage sensors are used in order to measure the output voltage of the inverter and the output voltage of each bridge, as illustrated in Fig. 5(f). Except getting the voltage shown in the figure, also get the upper and lower unit voltage, respectively, as the sample data.

As shown in Table I, the single-phase five-level cascaded H-bridge inverter OC faults fall into six broad categories, which include 37 classes. The first two categories of faults are called simple fault, which includes 9 classes, and the next four categories of faults are called complicated faults, which covers 28 classes. When the third or the fourth category faults occur, it causes the inverter breakdown quickly. Additional sensors and high cost may be required in order to be able to separate all the classes of these two categories. Hence, only the two broad categories are discussed afterwards. In this way, there are 33 classes of faults in this paper.

III. PCA-mRVM-Based Fault Diagnosis Strategy

Fig. 6 shows the structure of PCA-mRVM fault diagnosis strategy. In fact, the CHMLIS fault diagnosis is composed of four parts: feature extraction, classification diagnostic model, output diagnostic results, and switching pattern calculation. This paper mainly studies the first three parts. This section takes the simple fault as an example to introduce the strategy studied in this paper. First, the model would output the classification results in the form of binary code via the multinomial probit link $l_a = i$ if $y_{ai} > y_{aj}\ \forall j \neq i$ [34]. After that, the binary codes are compared with the prior knowledge to decode the faults type and location. The binary codes of simple faults are shown in Table II. For instance, the classification model output is $[0,1,0,0,0,0,0,0,0]^{\mathrm{T}}$ when a CHMLIS OC fault occurs at Bridge 1-Switch 1 (H1S1), as shown in Fig. 5(b) the classification model output $[0,1,0,0,0,1,0,0,0]^{\mathrm{T}}$ stands for two CHMLIS OC fault occurs at H1S1 and H2S1, as shown in Fig. 5(f). The other types of simple fault can be seen in Table II.

TABLE II
Fault Class and Labels

Fault class	label
Normal	$[1,0,0,0,0,0,0,0,0]^{\mathrm{T}}$
H1S1 Open	$[0,1,0,0,0,0,0,0,0]^{\mathrm{T}}$
H1S2 Open	$[0,0,1,0,0,0,0,0,0]^{\mathrm{T}}$
H1S3 Open	$[0,0,0,1,0,0,0,0,0]^{\mathrm{T}}$
H1S4 Open	$[0,0,0,0,1,0,0,0,0]^{\mathrm{T}}$
H2S1 Open	$[0,0,0,0,0,1,0,0,0]^{\mathrm{T}}$
H2S2 Open	$[0,0,0,0,0,0,1,0,0]^{\mathrm{T}}$
H2S3 Open	$[0,0,0,0,0,0,0,1,0]^{\mathrm{T}}$
H2S4 Open	$[0,0,0,0,0,0,0,0,1]^{\mathrm{T}}$

A. Signal Preprocessing Based on FFT

The output voltage waveforms are sampled from the CHMLIS prototype under no-load condition, as shown in Fig. 4. We can see that the signals are difficult to rate as an important characteristic for fault classification. Therefore, a signal transformation technique must be adopted. To be more precise, the choice of feature extraction method must supply sufficient fault details for classification model. One possible technique for implementation on a digital signal processing microchip is FFT. The FFT technique has a good identity feature to classify normal and abnormal features.

By sampling a period of a discrete output voltage signal $\{f_b\}_0^{B-1}$, the result data $X \in \Re^{A\times B}$ can be achieved after FFT, where A is the size of observations, B is the size of the selected previous harmonic. The FFT transformation is illustrated as (2) and (3) [32]. Then, the preprocessed fault data $X \in \Re^{A\times B}$ is corresponded to its category label as an input data υ, l is the category label of each fault

$$F_k = G_k + W_B^k H_k, \quad \text{for } k = 0,\ldots,\frac{B}{2}-1 \tag{2}$$

$$F_{k+B/2} = G_k - W_B^k H_k, \quad \text{for } k = 0,\ldots,\frac{B}{2}-1 \tag{3}$$

where $W_B = e^{-j2\pi/B}$, G_k is defined for even-numbered elements of f_b, whereas H_k is for odd-number elements of f_b. G_k and H_k can be computed by (4) and (5). Obviously, the results are satisfactory for identifying fault features

$$G_k = \sum_{b=0}^{\left(\frac{B}{2}\right)-1} f_{2b} W_{B/2}^{bk} \tag{4}$$

$$H_k = \sum_{b=0}^{\left(\frac{B}{2}\right)-1} f_{2b+1} W_{B/2}^{bk}. \tag{5}$$

In this paper, after getting voltage signal from the inverter, FFT is used to achieve signal preprocessing. By analyzing the operating principle of the inverter and the characteristics of FFT, it can be seen that when a fault of the switching devices at H1 (S1 and S2) or at H2 (S3 and S4) occurs simultaneously, the FFT data does not change, as well as the change of phase, which is equal to π. Thus, it is hard to distinguish the fault only by using the spectrum, as shown in Fig. 7. However, by

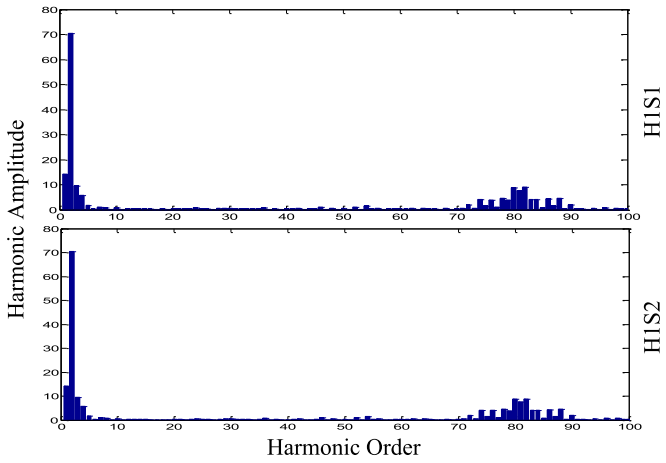

Fig. 7. Harmonics amplitude for H1S1 and H1S2 using FFT.

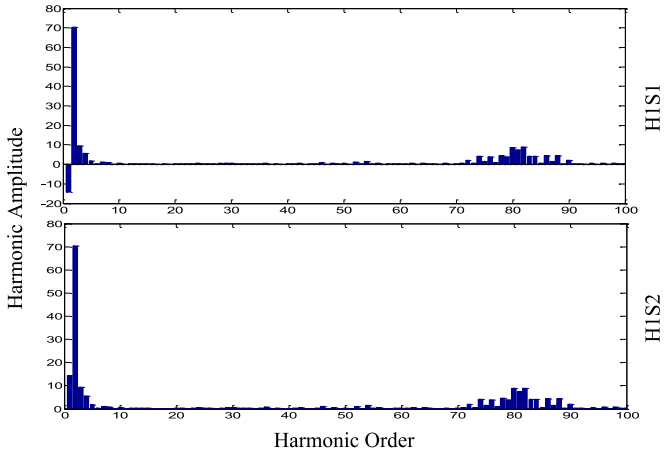

Fig. 8. Harmonics amplitude for H1S1 and H1S2 after special handling.

adding the phase information of the voltage data after FFT, the different characteristics of these two faults are separated. Hence, the sample dimension will be increased too. Considering these reasons, this paper will adopt the method that extracts the real part of the dc component, which can differentiate between these cases, as shown in Fig. 8.

B. Feature Extraction Based on PCA

The dimension of variables is till high after FFT. Therefore, it is difficult to list each feature for fault diagnosis classification. Basically, PCA is a statistical technique, which is used to transform a set of correlated variables to a new lower dimensional set of variables, which are uncorrelated or orthogonal with each other. A reduced representation of the original data is obtained, which is smaller but having enough information to deal with. The discussion of PCA presented in this section will be brief, providing only indispensable equations to elucidate the fundamental PCA approach applied to a fault diagnosis system in CHMLIS.

Suppose $X \in \Re^{A\times B}$ is a $A \times B$ data matrix of system variable sequence. Where the size of samples is A, the size of variables (that is the selected previous harmonic) is B. Then, the covariance matrix equation can be calculated from

$$R_X = E\left\{[X - E(X)]\,[X - E(X)]^T\right\}. \tag{6}$$

The eigenvalues λ and the corresponding eigenvectors P would be obtained by

$$|\lambda I - R_X| = 0 \tag{7}$$

$$|\lambda_i I - R_X|\, p_i = 0, i = 1, 2, \ldots, B \tag{8}$$

where the λ_i is the ith eigenvalue of R_X, and it can be arranged as $\lambda_1 \geq \lambda_2 \geq \ldots \geq \lambda_B$. p_i is the eigenvector of R_X corresponding to λ_i.

The size of principal components (PCs) is selected by cumulative percent variance (CPV), as shown in the following equation:

$$\mathrm{CPV}(m) = \left(\frac{\sum_{i=1}^{m}\lambda_i}{\sum_{i=1}^{B}\lambda_i}\right) \times 100\% \geq \mathrm{CL} \tag{9}$$

where the value of CL can be determined by the user as predetermined limit [33]. Finally, a new lower dimensional matrix $\tilde{X}$ can be calculated from

$$X = \mathrm{TP} = \sum_{i=1}^{B} t_i p_i^T = \sum_{i=1}^{m} t_i p_i^T + \sum_{i=m+1}^{B} t_i p_i^T = \tilde{X} + E \tag{10}$$

where T is the score matrix, P is the load matrix, t_i is the score vectors and p_i is the load vectors, and m is the dimension of the principal component space. m is much less than B. $\tilde{X}$ is the principal component matrix, E is the residual matrix. PCA reduces the original set of B variables to m principal components.

In this paper, after signal preprocessing based on FFT, the signals are converted from time domain to frequency domain. Such as matrix $X \in \Re^{A\times B}$ in (6), the size of variables B is the FFT harmonic order. Harmonic amplitude is used as the value of the variables. PCA method is used to transform the set of correlated dates to a new lower dimensional set, as matrix X to matrix $\tilde{X}$ in (10). The cumulative percent variance from PCA is selected around 85% to get appropriate principal components using (9).

C. mRVM Classification Method

Multiclass multikernel relevance vector machines (mRVMs) expand the original relevance vector machines (RVM) into the multiclass setting by introducing auxiliary variables Y, which act as intermediate regression targets, and which naturally lead to the multinomial probit likelihood [39] for the estimation of class membership probabilities. The auxiliary variables Y also provide significantly competitive results in contrast to the traditional classification approach [e.g., Suppot Vector Machine (SVM)]. In fact, it achieves sparsity without the constraint of having a binary class problem and provides probabilistic outputs for class membership instead of the hard binary decisions given by the traditional SVMs. In this paper, the mRVM algorithm is utilized to classify the faults after feature extraction. In

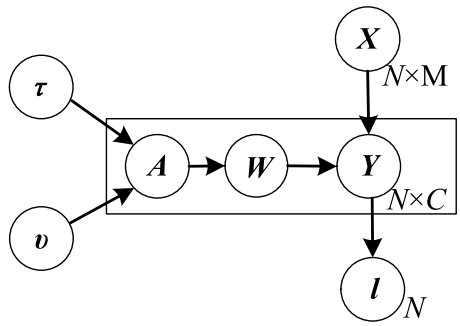

Fig. 9. Hierarchical Bayesian model.

the following, a brief introduction of mRVM and indispensable equations are given [34].

First, a training set $\{\tilde{x}_i, l_i\}_{i=1}^{A}$ should be given, where $\tilde{\mathbf{X}} \in \Re^{A \times m}$ is the samples dimension and $l \in \{1 \dots C\}$ is the class label. More conveniently, we derived our training kernel $\mathbf{K} \in \Re^{A \times A}$ based on a dataset-dependent kernel function from $\tilde{\mathbf{X}} \in \Re^{A \times m}$. The learning processes involve the inference of the model parameters $\mathbf{W} \in \Re^{A \times C}$, which by the quantity $\mathbf{W^T K}$ act as a voting system to express which relationships of the data are important in order to have appropriate discriminative properties for the model. Hereafter, the auxiliary variables $\mathbf{Y} \in \Re^{C \times A}$ act as the regression targets of $\mathbf{W^T K}$. This way, the standardized noise model can be calculated from

$$y_{ca}|w_c, k_a \sim \left(w_c^T k_a, 1\right). \tag{11}$$

As regressors $\mathbf{W}$ express the weight with which a data point "votes" for a specific class, the auxiliary variables Y express a class membership ranking system. Given a sample n, we assign it to the class c with the highest y_{cn}. The continuous nature of Y allows not only multiple class discrimination via the multinomial probit link $l_a = i$ if $y_{ai} > y_{aj}\ \forall j \neq i$ but also a probabilistic output for class membership via the resulting multinomial probit likelihood function

$$P\left(t_a = i|\mathbf{W}, \mathbf{k_a}\right) = \varepsilon_{p(u)}\left\{\prod_{j \neq i} \phi\left(u + \left(\mathbf{w_i} - \mathbf{w_j}\right)^T \mathbf{k_a}\right)\right\} \tag{12}$$

where $u \sim N(0,1)$ and ϕ are the Gaussian cumulative distribution function. The training procedure involves consecutive updates of the model parameters based on standard expectation maximization (E-M) scheme. The regressors $\mathbf{W}$ closed-form posterior can be calculated from Fig. 9

$$\begin{aligned} &P\left(\mathbf{W}|\mathbf{Y}\right) \propto P\left(\mathbf{Y}|\mathbf{W}\right) P\left(\mathbf{W}|\mathbf{A}\right) \\ &\propto \prod_{c=1}^{C} N\left(\left(\mathbf{KK^T} + \mathbf{A_c}\right)^{-1} \mathbf{Ky_c^T}, \left(\mathbf{KK^T} + \mathbf{A_c}\right)^{-1}\right) \end{aligned} \tag{13}$$

where $\mathbf{A_c}$ is the diagonal matrix derived from the c column of $\mathbf{A}$, which expresses the scales α_{ic} across samples. Based on the previous equations, the maximum a posteriori (MAP) estimator for the regressor is $\hat{\mathbf{W}} = \mathrm{argmax}_{\boldsymbol{w}} P\left(\mathbf{W}|\mathbf{Y}, \mathbf{A}, \mathbf{K}\right)$. Thus, the parameters update method is based on the MAP value as shown in the following equation:

$$\hat{\mathbf{w}}_\mathbf{c} = \left(\mathbf{KK^T} + \mathbf{A_c}\right)^{-1} \mathbf{Ky_c^T}. \tag{14}$$

The posterior distribution of the auxiliary variables can be calculated by (14) as well as [40]. In the case of $\forall c \neq i$, its E step is shown in the following equation:

$$\hat{y}_{ca} \leftarrow \hat{w}_c^{\mathrm{T}} k_a - \frac{\varepsilon_{P(u)}\left\{N_u\left(\hat{w}_c^T \mathrm{k}_a - \hat{w}_i^T k_a, 1\right) \Phi_u^{a,i,c}\right\}}{\varepsilon_{P(u)}\left\{\Phi\left(u + \hat{w}_i^{\mathrm{T}} k_a - \hat{w}_c^{\mathrm{T}} k_a\right) \Phi_u^{a,i,c}\right\}}. \tag{15}$$

As for the *i*th class, its E step is shown in the following equation:

$$\tilde{y}_{ia} \leftarrow \hat{w}_i^{\mathrm{T}} \mathrm{k}_a - \left(\sum_{j \neq i} \tilde{y}_{ja} - \hat{w}_j^{\mathrm{T}} k_a\right). \tag{16}$$

After the update of the hyperpriors α_{ac}, the closed-form posterior is shown in the following equation:

$$\begin{aligned} &P\left(\mathbf{A}|\mathbf{W}\right) \propto P\left(\mathbf{W}|\mathbf{A}\right) P\left(\mathbf{A}|\tau, \upsilon\right) \\ &\propto P \prod_{c=1}^{C} \prod_{a=1}^{A} G\left(\tau + \frac{1}{2}, \frac{w_{ac}^2 + 2\upsilon}{2}\right). \end{aligned} \tag{17}$$

The mean of Gamma distribution is shown in the following equation:

$$\tilde{\alpha}_{nc} = \frac{2\tau + 1}{w_{ac}^2 + 2\upsilon}. \tag{18}$$

The detail of the E-M scheme can be found in [34].

In this paper, after data dimension reduction based on PCA, mRVM is used for data classification. Data after PCA are assigned to $\tilde{x}_i$ in training set $\{\tilde{x}_i, l_i\}_{i=1}^{A}$. The class label $l \in \{1 \dots C\}$ is given in Table II. The Gaussian kernel function is used in the mRVM, and the parameter of the kernel function is selected by the accuracy of classification. After the data standardization, we select convergence criterion by trivial change in hyperproirs τ and υ, as shown in (17). In order to get higher model sparse degree for short diagnosis time, the mRVM limits most of the model parameters near zero based on the Bayesian framework using fast Type-II maximum likelihood method.

This paper employs the experimental data to validate the effectiveness of the proposed approach for the detection and diagnosis of the simple faults, while the simulation data are used in order to validate the performance of the proposed approach on complicated faults.

The PCA-mRVM strategy working process is shown in Fig. 10. The working process can be described as in the following:

- *Step 1:* Initializing the parameters of the PCA-mRVM strategy.
- *Step 2:* Inputting the experimental samples or simulation samples to diagnose.
- *Step 3:* Preprocessing the samples based on FFT by (4) and (5).
- *Step 4:* Extracting sample's feature based on PCA with (9) and (10), and setting the PCA parameters (CL). After PCA, the data are divided into two groups, one is

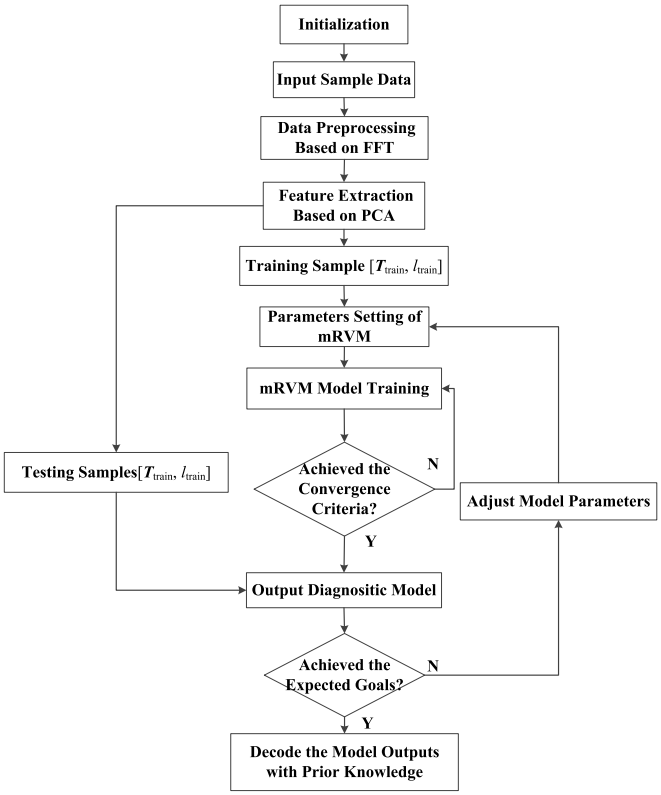

Fig. 10. Flow chart of the fault diagnosis strategy based on the PCA-mRVM strategy.

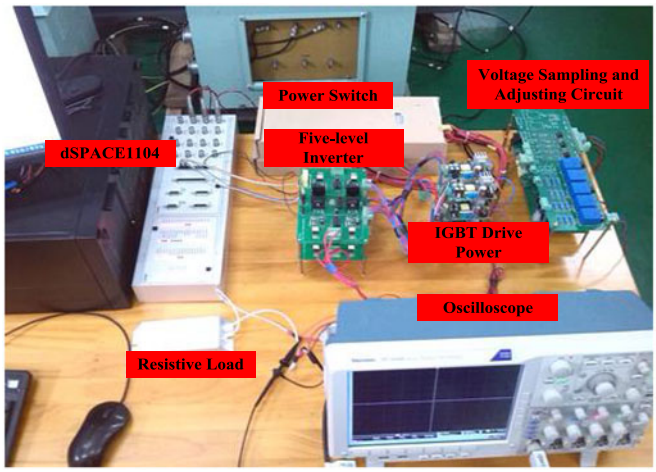

Fig. 11. Experimental setup.

training data and the other is test data. The training data are used to train the mRVM classification model and the test data are used to verify the effect of the classification.

Step 5: The samples that are extracted after Step 4 falls into training samples $[T_{\text{train}}, l_{\text{train}}]$ and testing samples $[T_{\text{test}}, l_{\text{test}}]$.

Step 6: Setting the kernel parameters for the mRVM model as shown in Figs. 12 and 15.

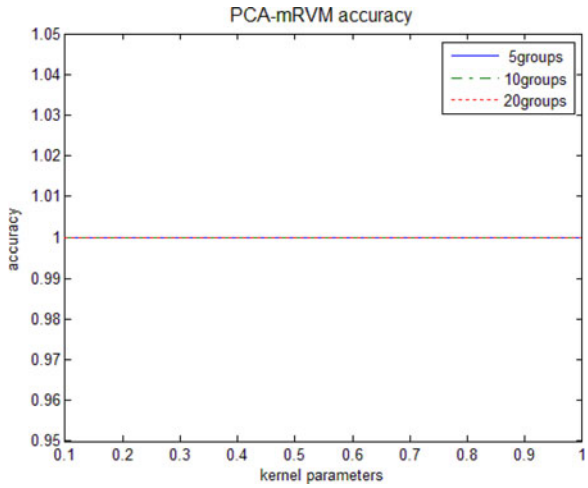

Fig. 12. Diagnosis accuracy along with the changing of mRVM kernel parameter for sample fault.

TABLE III
MAIN PARAMETERS OF THE SYSTEM

Symbol	Quantity	Value
U_{dc}	dc-link voltage	48 V
R_{load}	Resistance load	1 kΩ
f_s	switching frequency	1 kHz
f_{esample}	Experimental sample frequency	25 kHz
f_{ssample}	Simulation sample frequency	40 kHz

Step 7: Modeling learning process. Calculating relevance vector based on training samples. If the convergence criterion is unsatisfied, then go back to retrain the relevance vector, else output the diagnostic model.

Step 8: The testing samples are utilized to test the diagnosis performance of diagnostic model. If the diagnosis performance achieves expected goals, then decode the model outputs with prior knowledge, else go back Step 6 to adjust the parameters.

IV. EXPERIMENTAL TESTS

According to the single-phase cascaded five-level inverter principle shown in Fig. 2, the CHMLIS fault diagnosis experimental has been built based on dSPACE1104 control system, the main parameters of the system are set as shown in Table III. The experimental circuit structure is shown in Fig. 11, wherein the drive circuit consists of integrated power modules TLP250. The *N*-channel power IGBT IRGP35B60PD is selected as the power switch transistors in this system, which includes a built-in reverse diode. One voltage sensor is used to measure the output voltage of the system. Two switching power supplies S-480-48 are selected as switch powers, which input 115V-230V/ac and output +48V/dc. This single-phase CHMLIS is controlled by carrier phase-shifted SPWM (CPS-SPWM).

TABLE IV
PARAMETER CONFIGURATION FOR DIFFERENT METHODS

Methods	PCs	Parameter Configuration
PCA-BP	2	$innum = 2$, $midnum = 8$, $outnum = 9$, $f(x) = \frac{1}{1+e^{-x}}$, $\eta = 0.01$.
PCA-SVM	2	$\mathbf{K}(x,y) = \exp\left(-\frac{\|x-y\|^2}{2\sigma^2}\right)$, $CL = 0.85$, $c = 5$, $\sigma = 0.02$
PCA-mRVM	2	$\mathbf{K}(x,y) = \exp\left(-\frac{\|x-y\|^2}{2\sigma^2}\right)$, $CL = 0.85$, $\sigma = 0.5$.

TABLE V
COMPARISON OF GAUSSIAN KERNEL AND LINEAR KERNEL IN TESTING TIME AND DIAGNOSIS ACCURACY ON SIMPLE FAULT

Testing samples(groups)	Average testing time (s)		Average diagnosis accuracy (%)	
	Gaussian kernel $\sigma = 0.5$	Linear kernel	Gaussian kernel $\sigma = 0.5$	Linear kernel
5	0.012756	0.0130622	100	100
10	0.013735	0.0117653	100	100
20	0.01105	0.0099956	100	100

A. Workflow Diagram of Fault Diagnosis

Fig. 6 presents the main workflow of the single-phase cascaded H-bridge five-level inverter fault diagnosis experimental. The construction is based on dSPACE1104 real-time control system. The inverter experimental circuit covers dead-zone circuit, driving circuit as well as H-bridge main circuit. The SC faults are generally converted into OC faults by implanting rapidly fuses into the inverter circuit. Hence, we focus on OC faults in CHMLIS.

B. Parameters Setting

In order to verify the effectiveness of the PCA-mRVM strategy, the traditional approaches, such as BP neural network, SVM, are applied for CHMLIS fault diagnosis. In this section, the simple fault is validated by the experimental data. There exist 50 groups of samples after FFT transformation; each group has nine classes of faults. The fault category labels are shown in Table II. The sampling frequency is 25 kHz, sampling time is 0.02 s, so the size of samples is 500. The sampled output voltage signals harmonics are computed using the FFT. The FFT waveform is symmetrical in one cycle, only the first half cycle is utilized for classification. Depending on the single OC fault location, the inverter output voltage is different as illustrated in Fig. 4. The output voltage waveforms are nearly the same when the faults appear at the same position. Thus, only the inverter output voltage, which is measured by voltage sensor, is utilized to diagnosis simple fault. The training samples are 30 groups of samples $[\tilde{T}_{\text{train}}, \tilde{l}_{\text{train}}]^{270 \times 250}$, which are selected from the original experimental samples of 50 groups. The testing samples are selected from the remaining 20 groups and contain 5 groups $[\tilde{T}_{\text{test}}, \tilde{l}_{\text{test}}]^{45 \times 250}$, 10 groups $[\tilde{T}_{\text{test}}, \tilde{l}_{\text{test}}]^{90 \times 250}$, and 20 groups $[\tilde{T}_{\text{test}}, \tilde{l}_{\text{test}}]^{180 \times 250}$. Since the features of these samples are too large to deal with, it is necessary to reduce the dimension of the samples. Hence, PCA is utilized to reduce the dimension of the samples after FFT computation. It allows extracting features of complex numbers and simplifies samples by introducing relative operators. After training 50 times, the average parameter configuration is shown in Table IV.

Herein, the $innum$ means the size of input layer, $midnum$ means the size of output layer. $f(x)$ is the transfer function in hidden layer, η is the learning rate. For better performance, the parameters of the PCA-BP method are selected according to experience. $\mathbf{K}(x, y)$ is the kernel function and σ is the kernel parameter for several methods. c is the penalty factor of SVMs, CL is the predetermined limit for PCA. The value of CL is 0.85, which can extract the characteristics of the data under the cumulative percent variance from PCA. Based on (9), the number of PCs is decided according to CL. The parameter of kernel function is selected by the accuracy of classification. As shown in Table V, in simple fault diagnosis, the average testing time when using linear kernel is shorter than using Gaussian kernel ($\sigma = 0.5$), and the average diagnostic accuracy is 100% in both kernel functions. It is shown that linear kernel function is a little better for simple fault diagnosis in testing time. But in the analysis of diagnosis accuracy of more complicated fault, Gaussian kernel function is much better than linear kernel. Therefore, Gaussian kernel function is selected.

Fig. 12 shows the diagnosis accuracy changing along with mRVM kernel parameter for different test sample groups (5, 10, and 20 groups). Gaussian kernel function is used in mRVM and the range of used parameters is (0, 1). As shown in Fig. 12, with the increase of kernel parameters, fault diagnosis accuracy is 100%. Therefore, mRVM kernel parameter of fault diagnosis model is initialized to 0.5.

C. Comparison and Analysis

The relevant vectors variation of the PCA-mRVM strategy during training process is shown in Fig. 13. In the process of iterative learning, most of the parameters of the posterior distribution tends to zero and has nothing to do with forecast. The nonzero parameter corresponding point is called the relevance vector that reflects the characteristics of the training data. After 300 iterations, the relevant vectors are obviously reduced. This means that the data sparsity is reduced with the increase of iteration steps by the mRVM approach. Hence, the proposed strategy could achieve higher model sparsity and shorter diagnosis time.

As expected, PCA conveys lower dimensional input space, which greatly reduced the time of the model training. Moreover, the noise reduction could improve the mapping performance, which leads to the improvement of total classification performance. As shown in Table VI, the PCA-BP has the longest testing time, and its diagnostic accuracy is the lowest of these

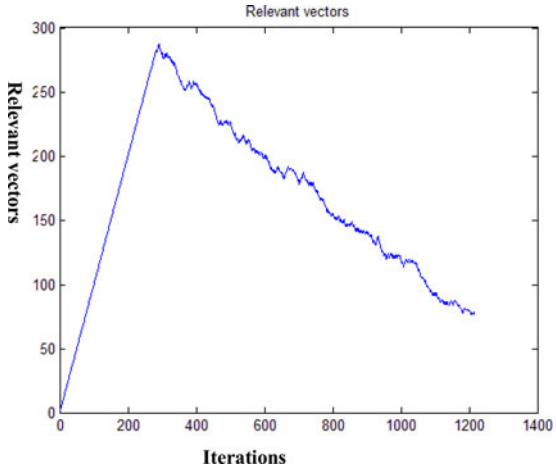

Fig. 13. Relevant vectors during training process.

TABLE VI
EXPERIMENTAL RESULTS OF FAULT DIAGNOSIS BASED ON DIFFERENT METHODS.

	Average testing time (s)			Average diagnosis accuracy (%)		
Testing samples (groups)	PCA -BP	PCA-SVM	PCA-mRVM	PCA-BP	PCA-SVM	PCA-mRVM
5	0.076	0.068	0.047	85.63	100	100
10	0.103	0.071	0.052	86.21	97.2	100
20	0.122	0.083	0.056	78.31	96.5	100

	Normal	H1S1	H1S2	H1S3	H1S4	H2S1	H2S2	H2S3	H2S4	
$Q=$	0.9749	0.0140	0.0107	0.0001	0.0003	0.0000	0.0000	0.0000	0.0000	Normal
	0.0020	0.9851	0.0065	0.0000	0.0055	0.0009	0.0000	0.0000	0.0000	H1S1
	0.0001	0.0179	0.9570	0.0012	0.0000	0.0006	0.0231	0.0000	0.0000	H1S2
	0.0000	0.0000	0.0024	0.9897	0.0000	0.0000	0.0000	0.0079	0.0000	H1S3
	0.0000	0.0018	0.0000	0.0000	0.9958	0.0000	0.0000	0.0000	0.0024	H1S4
	0.0000	0.0002	0.0000	0.0000	0.0000	0.8515	0.0154	0.0000	0.1329	H2S1
	0.0000	0.0000	0.0000	0.0000	0.0000	0.0269	0.8654	0.1077	0.0000	H2S2
	0.0000	0.0000	0.0003	0.0005	0.0000	0.0000	0.1821	0.8172	0.0000	H2S3
	0.0000	0.0003	0.0000	0.0000	0.0006	0.1826	0.0000	0.0000	0.8165	H2S4

Fig. 14. Probabilistic outputs of PCA-mRVM model.

approaches. Although PCA-SVM has a similar average diagnostic accuracy rate compared with the PCA-mRVM strategy, the latter could achieve higher model sparsity and could overcome the problem of binary class constraint.

Furthermore, PCA-mRVM can provide probabilistic outputs for each membership class instead of hard binary decisions given by PCA-SVM. This feature should be very useful in further study of failure characteristics and fault-tolerant control, which would give the detail of fault information and provide the damage probability of each device. The probabilistic outputs of the PCA-mRVM strategy has been illustrated in Fig. 14. According to the multinomial probit link $l_a = i$ if $y_{ai} > y_{aj}\ \forall j \neq i$, the maximum value of each column means which category it belongs to. The probabilistic outputs have a good theoretical guidance and practical significance for further research of fault diagnosis. For example, from the last column of Fig. 14, the value of $Q(9,6)$is lower than $Q(9,9)$, while it is higher than other rows. Thus, we can assume that there are some relationships between the two rows. Since we know that the $Q(9,6)$ refers to the probability of H2S1 OC fault, and the $Q(9,9)$ refers to the probability of H2S4 OC fault. Actually, the fault signature of H2S1 is more similar with H2S4 than the others. Compared with PCA-SVM, PCA-mRVM cannot only reduce the running time but also achieves the probabilistic outputs of each fault. The experimental results have achieved the expected goals and verified the correctness and effectiveness of the PCA-mRVM strategy.

V. SIMULATION RESULTS FOR COMBINED FAULTS

To verify the effectiveness and the diagnosis performance of the proposed strategy, all combined faults are tested on the model of a single-phase five-level cascaded H-bridge inverter. Simulation results indicate that the modified fault diagnosis method not only has a good performance in the single fault classification, but has also good performance in complicated faults. To test the fault diagnosis performance of the PCA-mRVM strategy, a 10% white Gaussian noise was added to the simulation samples. The related simulation parameters are as follows: the modulation index m_a is set as 0.8 out of 1.0, the sampling frequency f is 40 kHz and the size of samples is 800. The driven signals are the same as the experiment. The sampled output voltage signals harmonics are computed using the FFT. As discussed earlier, it is difficult to distinguish the complicated faults by means of the output voltage of the system. Hence, three voltage sensors have been used in order to retrieve the inverter output voltage and the output voltage of each bridge. As described in Section II, there are 33 classes of faults in the simulation samples.

A. Parameters Setting

In this section, complicated faults are classified based on different methods using simulation data. There are 60 groups of samples after FFT transformation. Each group has 33 classes of faults. The training samples category labels will be set by prior knowledge and the original data samples could be achieved after FFT computation. The previous paragraph has introduced the processes of generating simulation samples. The training samples are 40 groups of samples $[T_{\text{train}}, l_{\text{train}}]^{1320 \times 1200}$, which are selected from the original simulation samples of 60 groups. The testing samples are selected from the remaining 20 groups as follows: 5 groups$[T_{\text{test}}, l_{\text{test}}]^{165 \times 1200}$, 10 groups $[T_{\text{test}}, l_{\text{test}}]^{330 \times 1200}$, and 20 groups $[T_{\text{test}}, l_{\text{test}}]^{660 \times 1200}$. It is known that the original samples consist of three parts, and each part has 400 features extracted using FFT. The proposed approach for data preprocessing in this section is the same as the previous experimental validation. After training 50 times, the parameters configuration are given in Table VII .

As shown in Table VIII, in simple fault diagnosis, the average testing time using linear kernel is shorter than the one when using Gaussian kernel in parameter ($\sigma = 0.5$). However, the average diagnosis accuracy of Gaussian kernel is around 96% in comparison to the linear kernel one that is 59%. It is, therefore, shown that the average diagnostic accuracy of Gaussian kernel

TABLE VII
PARAMETER CONFIGURATION OF DIFFERENT METHODS

Methods	PCs	Parameter Configuration
PCA-BP	8	$innum = 60$, $midnum = 37$, $outnum = 33$, $f(x) = \frac{1}{1+e^{-x}}$, $\eta = 0.01$.
PCA-SVM	8	$\mathbf{K}(x,y) = \exp\left(-\frac{\|x-y\|^2}{2\sigma^2}\right)$, $CL = 0.85$, $c = 5$, $\sigma = 0.002$.
PCA-mRVM	8	$\mathbf{K}(x,y) = \exp\left(-\frac{\|x-y\|^2}{2\sigma^2}\right)$, $CL = 0.85$, $\sigma = 0.5$.

TABLE VIII
COMPARISON OF GAUSSIAN KERNEL AND LINEAR KERNEL

	Average testing time (s)		Average diagnosis accuracy (%)	
Testing samples (groups)	Gaussian kernel $\sigma = 0.5$	Linear kernel	Gaussian kernel $\sigma = 0.5$	Linear kernel
5	0.24185692	0.240744696	97.30	59.39
10	0.217535992	0.208692854	98.11	56.67
20	0.19784493	0.185974124	97.97	54.85

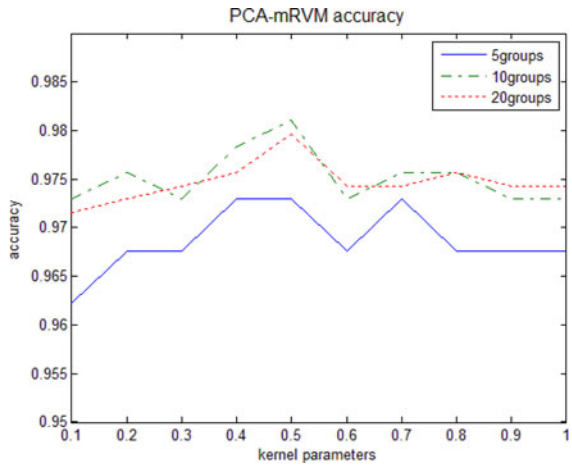

Fig. 15. Diagnostic accuracy of complicated faults with the changing of mRVM kernel parameter.

function is much better than the linear kernel one for complicated faults diagnosis. Therefore, Gaussian kernel function is adopted for the proposed PCA-mRVM strategy.

Fig. 15 shows the diagnosis accuracy versus the mRVM kernel parameter for different test sample groups (5, 10, and 20 groups). The Gaussian kernel function is used in the mRVM, kernel parameters is (0, 1) allowing easiest data processing. With the increase of kernel parameters, the fault diagnosis accuracy changes from 0.9650 to 0.9811. As the parameters of the Gaussian kernel function is selected within a certain range, the mRVM kernel parameters of the fault diagnosis model is initialized to 0.5, which make the accuracy of 5 and 10 groups

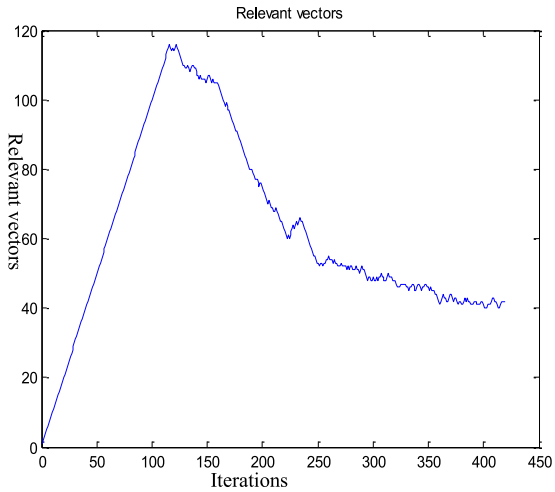

Fig. 16. Relevant vectors during training process.

TABLE IX
SIMULATION RESULTS OF CIRCUIT FAULT DIAGNOSIS BASED ON SEVERAL METHODS

	The average testing time (s)			The average diagnosis accuracy (%)		
Testing samples (groups)	PCA -BP	PCA-SVM	PCA-mRVM	PCA -BP	PCA-SVM	PCA-mRVM
5	1.342	0.133	0.120	81.32	98.66	97.30
10	1.571	0.139	0.131	80.54	93.25	98.11
20	1.588.	0.145	0.137	78.11	92.78	97.97

to be the highest, and the accuracy of the 20 groups to have better performance.

B. Comparison and Analysis

The average fault diagnosis results of these approaches are shown in Table VII. The relevant vectors variation of the PCA-mRVM strategy during the training process is shown in Fig. 16. After 100 iterations, relevant vectors are obviously reduced during the training process. This means that data sparsity is reduced with the increase of iteration steps by the mRVM approach. Hence, the proposed strategy could achieve higher model sparsity and shorter diagnosis time.

As it can be seen from Table IX, the PCA-mRVM fault diagnosis strategy has achieved the best diagnosis performance. Due to its shortest testing time, the PCA-mRVM could achieve highest model sparsity without the constraint of having a binary class problem. In addition of that, it could provide probabilistic outputs for class membership instead of the hard binary decisions given by the SVMs. The PCA-mRVM strategy not only reaches the highest accuracy rate which is almost 100%, but its computing time is the shortest among these approaches. The simulation results have achieved the expected goals. These results have verified the correctness and the effectiveness of the PCA-mRVM based strategy.

VI. Conclusion

This paper dealt with cascaded H-bridge multilevel inverter systems fault diagnosis. In this context, a fault diagnosis strategy based on a PCA-mRVM has been proposed. The proposed approach has been evaluated and validated on experimental data issued from a CHMLIS controlled using a dSPACE1104 real-time system. Based on the knowledge of the inverter behaviors, its output voltage signals have been selected as fault characteristic ones for the fault diagnosis strategy. The main objectives for this strategy are as follows: 1) some distinct features are identified by signal preprocessing based on FFT; 2) fault diagnosis efficiency is increased by dimension reduction based on PCA; 3) diagnosis accuracy is improved by mRVM, which outputs the results of classification in the form of binary codes. Compared with PCA-BP and PCA-SVM, the achieved results obviously prove the proposed PCA-mRVM fault diagnosis strategy superiority over traditional approaches. Simulation and experimental results have shown that this strategy could not only reduce the running time but also achieves probabilistic outputs of each fault. It has a good theoretical guidance and practical significance for further investigations on fault diagnosis.

References

[1] J. Mathew, K. Mathew, N.A. Azeez, P.P. Rajeevan, and K. Gopakumar, "A Hybrid multilevel inverter system based on dodecagonal space vectors for medium voltage IM drives," *IEEE Trans. Power Electron.*, vol. 28, no. 8, pp. 3723–3732, Aug. 2013.

[2] H. Sheng, F. Wang, and C. W. Tipton IV, "A fault detection and protection scheme for three-level DC–DC converters based on monitoring flying capacitor voltage," *IEEE Trans. Power Electron.*, vol. 27, no. 2, pp. 685–697, Feb. 2012.

[3] S. Mariethoz, "Systematic design of high-performance hybrid cascaded multilevel inverters with active voltage balance and minimum switching losses," *IEEE Trans. Power Electron*, vol. 28, no. 7, pp. 3100–3113, Jul. 2013.

[4] M. F. Kangarlu and E. Babaei, "A generalized cascaded multilevel inverter using series connection of submultilevel inverters," *IEEE Trans. Power Electron.*, vol. 28, no. 2, pp. 625–636, Feb. 2013.

[5] J. F. Liu, K. W. E. Cheng, and Y. M. Ye, "A cascaded multilevel inverter based on switched-capacitor for high-frequency AC power distribution system," *IEEE Trans. Power Electron*, vol. 29, no. 8, pp. 4219–4230, Aug. 2014.

[6] M. R. Islam, Y. G. Guo, and J. G. Zhu, "A high-frequency link multilevel cascaded medium-voltage converter for direct grid integration of renewable energy systems," *IEEE Trans. Power Electron.*, vol. 29, no. 8, pp. 4167–4182, Aug. 2014.

[7] F. Khoucha, S. M. Lagoun, A. Kheloui, and M. E. H. Benbouzid, "A comparison of symmetrical and asymmetrical three-phase H-bridge multilevel inverter for DTC induction motor drives," *IEEE Trans. Energy Convers.*, vol. 26, no. 1, pp. 64–72, Mar. 2011.

[8] X. She, A. Q. Huang, T. Zhao, and G. Wang, "Coupling effect reduction of a voltage-balancing controller in single-phase cascaded multilevel converters," *IEEE Trans. Power Electron*, vol. 27, no. 8, pp. 3530–3543, Aug. 2012.

[9] S. M Jung, J. S. Park, H. W. Kim, K. Y. Cho, and M. J. Youn, "An MRAS-based diagnosis of open-circuit fault in PWM voltage -source inverters for PM synchronous motor drive systems," *IEEE Trans. Power Electron.*, vol. 28, no. 5, pp. 2514–2526, May 2013.

[10] M. Salehifar, R. S. Arashloo, J. M. Moreno-Equilaz, V. Sala, and L. Romeral, "Fault detection and fault tolerant operation of a five phase PM motor drive using adaptive model identification approach," *IEEE J. Emerg. Sel. Topics Power Electron*, vol. 2, no. 2, pp. 212–223, Jun. 2014.

[11] X. J. Pei, S. S. Nie, Y. Chen, and Y. Kang, "Open-circuit fault diagnosis and fault-tolerant strategies for full-bridge DC–DC converters," *IEEE Trans. Power Electron.*, vol. 27, no. 5, pp. 2550–2565, May 2012.

[12] U. M. Choi, H. G. Jeong, K. B. Lee, and F. Blaabjerg, "Method for detecting an open-switch fault in a grid-connected NPC inverter system," *IEEE Trans. Power Electron.*, vol. 27, no. 6, pp. 2726–2739, Jun. 2012.

[13] E. Ribeiro, A. J. M. Cardoso, and C. Boccaletti, "Open-circuit fault diagnosis in interleaved DC–DC converters," *IEEE Trans. Power Electron.*, vol. 29, no. 6, pp. 3091–3102, Jun. 2014.

[14] M. F. Kangarlu and E. Babaei, "A generalized cascaded multilevel inverter using series connection of submultilevel inverters," *IEEE Trans. Power Electron.*, vol. 28, no. 2, pp. 625–636, Feb. 2013.

[15] H. Wang, M. Liserre, F. Blaabjerg, P. de Place Rimmen, J. B. Jacobsen, T. Kvisgaard, and J. Landkildehus, "Transitioning to physics-of-failure as a reliability driver in power electronics," *IEEE J. Emerg. Sel. Topics Power Electron.*, vol. 2, no. 1, pp. 97–114, Mar. 2014.

[16] R. R. Errabelli and P. Mutschler, "Fault-tolerant voltage source inverter for permanent magnet drives," *IEEE Trans. Power Electron.*, vol. 27, no. 2, pp. 500–508, Feb. 2012.

[17] S. Khomfoi and L. M. Tolbert, "Fault diagnostic system for a multilevel inverter using a neural network," *IEEE Trans. Power Electron.*, vol. 22, no. 3, pp. 1062–1069, May. 2007.

[18] C. Delpha, C. Hao, and D. Diallo, "SVM based diagnosis of inverter fed induction machine drive: A new challenge," in *Proc. 38th Annu. Conf. IEEE Ind. Electron. Soc.*, 2012, pp. 3931–3936.

[19] H. G. Sheng, F. Wang, and C. W. Tipton, "A fault detection and protection scheme for three-level DC–DC converters based on monitoring flying capacitor voltage," *IEEE Trans. Power Electron.*, vol. 27, no. 2, pp. 685–697, Feb. 2012.

[20] P. G. Potamianos, E. D. Mitronikas, and A. N. Safacas, "Open-circuit fault diagnosis for matrix converter drives and remedial operation using carrier-based modulation methods," *IEEE Trans. Ind. Electron.*, vol. 61, no. 1, pp. 531–545, Jan. 2014.

[21] A. S. S. Vasan, B. Long, and M. Pecht, "Diagnostics and prognostics method for analog electronic circuits," *IEEE Trans. Ind. Electron.*, vol. 60, no. 11, pp. 5277–5291, Nov. 2013.

[22] N. M. A. Freire, J. O. Estima, and A. J. Marques Cardoso, "Open-circuit fault diagnosis in PMSG drives for wind turbine applications," *IEEE Trans. Ind. Electron.*, vol. 60, no. 9, pp. 3957–3967, Sep. 2013.

[23] S. Shao, P. W. Wheeler, J. C. Clare, and A. J. Watson, "Fault detection for modular multilevel converters based on sliding mode observer," *IEEE Trans. Power Electron.*, vol. 28, no. 11, pp. 4867–4872, Nov. 2013.

[24] A. B. Youssef, S. K. El Khil, and I. Slama-Belkhodja, "State observer-based sensor fault detection and isolation, and fault tolerant control of a single-phase PWM rectifier for electric railway traction," *IEEE Trans. Power Electron.*, vol. 28, no. 12, pp. 5842–5853, Dec. 2013.

[25] S. Khwan-on, L. de Lillo, L. Empringham, and P. Wheeler, "Fault-tolerant matrix converter motor drives with fault detection of open switch faults," *IEEE Trans. Ind. Electron.*, vol. 59, no. 1, pp. 257–268, Jan. 2012.

[26] A. Mohammadpour, S. Sadeghi, and L. Parsa, "A generalized fault-tolerant control strategy for five-phase PM motor drives considering star, pentagon, and pentacle connections of stator windings," *IEEE Trans. Ind. Electron.*, vol. 61, no. 1, pp. 63–75, Jan. 2014.

[27] J. Seshadrinath, B. Singh and B. K. Panigrahi, "Investigation of vibration signatures for multiple fault diagnosis in variable frequency drives using complex wavelets," *IEEE Trans. Power Electron.*, vol. 29, no. 2, pp. 936–945, Feb. 2014.

[28] P. Bordignon, M. Carpaneto, M. Marchesoni, and P. Tenca, "Faults analysis and remedial strategies in high power neutral point clamped converters," in *Proc. IEEE Power. Electron. Spec. Conf.*, 2008, pp. 2778–2783.

[29] G. Yufan, S. Dan, and H. Yikang, "Mean current vector based online real-time fault diagnosis for voltage source inverter fed induction motor drives," in *Proc. 7th IEEE Int. Electr. Mach. Drive. Conf.*, 2007, pp. 1114–1118.

[30] T. Jing, H. Yun'an, L. Tao, and C. Yu, "Analog circuit fault diagnosis based on fuzzy support vector machine and kernel density estimation," in *Proc. 3rd Int. Conf. Adv. Comput. Theory. Eng.*, 2010, pp. V4-544–V4-548.

[31] B. G. Jo and M. H. Sunwoo, "New continuous-flow mixed-radix (CFMR) FFT Processor using novel in-place strategy," *IEEE Trans. Circuit Syst. I, Reg. Papers*, vol. 52, no. 5, pp. 911–919, May 2005.

[32] S. Khomfoi and L. M. Tolbert, "Fault diagnostic system for a multilevel inverters using a neural network," *IEEE Trans. Power Electron.*, vol. 22, no. 3, pp. 1062–1069, May 2007.

[33] W. Chenglin, H. Jing, W. Tianzhen, and C. Zhiguo, "Relative PCA with applications of data compression and fault diagnosis," *Acta. Autom. Sin.*, vol. 34, pp. 1128–1139, 2008.

[34] I. Psorakis, T. Damoulas, and M.A. Girolami, "Multiclass relevance vector machines: Sparsity and accuracy," *IEEE Trans. Neural Netw.*, vol. 21, no. 10, pp. 1588–1598, Oct. 2010.

[35] T. Yu, X. Shaojun, and D. Jiudong, "Pulsewidth modulation of Z-source inverters with minimum inductor current ripple," *IEEE Trans. Ind. Electron.*, vol. 61, no. 1, pp. 98–106, Jan. 2014.
[36] S. Thielemans, A. Ruderman, B. Reznikov, and J. Melkebeek, "Improved natural balancing with modified phase-shifted PWM for single-leg five-level flying-capacitor converters," *IEEE Trans. Power Electron.*, vol. 27, no. 4, pp. 936–945, Apr. 2014.
[37] V. Choqueuse, M. E. H. Benbouzid, Y. Amirat, and S. Turri, "Diagnosis of three-phase electrical machines using multidimensional demodulation techniques," *IEEE Trans. Ind. Electron.*, vol. 59, no. 4, pp. 2014–2023, Apr. 2012.
[38] S. Karimi, A. Gaillard, P. Poured, and S. Saadate, "FPGA-based real-time power converter failure diagnosis for wind energy conversion systems," *IEEE Tran. Ind. Electron.*, vol. 55, no. 12, pp. 4299–4308, Dec. 2008.
[39] J. H. Albert and S. Chib, "Bayesian analysis of binary and polychotomous response data," *J. Amer. Statist. Assoc.*, vol. 88, no. 6, pp. 669–679, Jun. 1993.
[40] T. Damoulas and M. A. Girolami, "Combining feature spaces for classification," *Pattern Recog.*, vol. 42, no. 11, pp. 2671–2683, Nov. 2009.

Tianzhen Wang was born in Qingdao, China, in 1978. She received the B.Eng. and Ph.D. degrees in electrical engineering from the Shanghai Maritime University, Shanghai, China, in 2006, respectively.

She was a Postdoctoral Researcher in Naval Academy Research Institute of France, Brest, France, from 2007 to 2008. Since 2006, she has been with the Department of Electrical Engineering, Shanghai Maritime University, where she is currently an Associate Professor. Her research interests include fault detection and diagnosis methods and intelligent information processing.

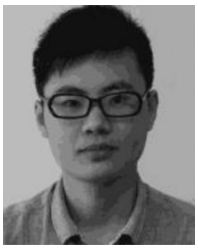

Hao Xu received the M.Tech. degree in electrical engineering from Shanghai Maritime University, Shanghai, China, in 2014.

His research interests include fault detection and diagnosis of multilevel inverter.

Jingang Han received the B.Eng. and Ph.D. degrees in electrical engineering from the Shanghai Maritime University, Shanghai, China, in 2001 and 2007, respectively.

Since 2007, he has been with the Department of Electrical Automation, Shanghai Maritime University, as an Associate Professor. From 2011 to 2012, he was a Postdoctoral Research Fellow at the French Naval Academy, Brest, France. His research interests include analysis, design, and control of power converter, multilevel converter and renewable energy applications.

Elhoussin Elbouchikhi (M'04) was born in Khemisset, Morocco, in 1987. He received the Diploma Engineer degree (Dipl.-Ing.) in automatic and electrical engineering, the Research Master's degree in automatic systems, computer science and decision from the National Polytechnic Institute of Toulouse, Toulouse, France, in 2010, and the Ph.D. degree from the University of Brest, Brest, France, in 2013.

He was a Postdoctoral Researcher at ISEN of Brest, Brest, France, from October 2013 to September 2014, where he is currently an Associate Professor and a Research Affiliate of the LBMS_lab. His current research interests include electrical machines fault detection and diagnosis.

Mohamed El Hachemi Benbouzid (S'92–M'95–SM'98) was born in Batna, Algeria, in 1968. He received the B.Sc. degree in electrical engineering from the University of Batna, Batna, Algeria, in 1990, the M.Sc. and Ph.D. degrees in electrical and computer engineering from the National Polytechnic Institute of Grenoble, Grenoble, France, in 1991 and 1994, respectively, and the Habilitation à Diriger des Recherches degree from the University of Picardie "Jules Verne," Amiens, France, in 2000.

After receiving the Ph.D. degree, he joined the Professional Institute of Amiens, University of Picardie "Jules Verne," where he was an Associate Professor of electrical and computer engineering. Since September 2004, he has been with the Institut Universitaire de Technologie of Brest, University of Brest, Brest, France, where he is a Professor of electrical engineering. His main research interests and experience include analysis, design, and control of electric machines, variable-speed drives for traction, propulsion, and renewable energy applications, and fault diagnosis of electric machines.

Prof. Benbouzid is the Editor-in-Chief of the *International Journal on Energy Conversion* (IRECON). He is also an Associate Editor of the IEEE TRANSACTIONS ON ENERGY CONVERSION, the IEEE TRANSACTIONS ON INDUSTRIAL ELECTRONICS, the IEEE TRANSACTIONS ON SUSTAINABLE ENERGY, and the IEEE TRANSACTIONS ON VEHICULAR TECHNOLOGY. He was an Associate Editor of the IEEE/ASME TRANSACTIONS ON MECHATRONICS from 2006 to 2009.